Mechanical Performance of Three Types of Connections Used in Orthogonal Ribbed Beams Made of Poplar Laminated Veneer Lumber

Yan Liu,[a,]* Jing Chen,[a] Hongwei Ma,[a,]* Meng Gong,[b] and Linfeng Zhang [a]

This study elucidated the mechanical performance of different connections used in orthogonal ribbed beams made of poplar laminated veneer lumber (LVL). Three types of connections (namely, U-, T-, and L-shape) were fabricated and used to connect the second beam and the middle part of a main beam to form an orthogonal rib beam. A concentrated load was applied to the intersection between the main beam and the second beam. The results showed: (1) all three types of ribbed beam connection specimens showed good connecting performance and the ductile failure, including the pull-out of partial self-tapping screws, crushing of LVL at the end of the ribbed beam, and connection failure; (2) the variation of load capacity of JD2-type specimens was approximately 3.2%, which was smaller than that of the JD1- and JD3-type specimens, slightly less than 10%; (3) the ultimate bearing capacity of a connection specimen was proportional to the number of self-tapping screws; and (4) the mechanical performance of the U-shaped connection specimens was worse than that of the L-and T-shaped connection specimens. The L-shaped connection was recommended due to its better mechanical performance, simpler configuration, and more convenient fabrication.

*Contact information: a: College of Civil Engineering, Yangzhou University, Yangzhou, Jiangsu 225127 P. R. China; b: Wood Science and Technology Center, University of New Brunswick, Fredericton, New Brunswick E3C 2G6 Canada; *Corresponding authors: hwma@yzu.edu.cn; liuyan@yzu.edu.cn*

INTRODUCTION

Laminated veneer lumber (LVL) is a new type of building material made of fast-growing poplar wood veneer and adhesives (Liu *et al.* 2013; Xiong *et al.* 2018). With the proper selection of the wood veneer, layups, adhesive type, and hot-press bonding parameters, adhesively laminated wood products can be designed and manufactured to meet the needs of human beings. Many scholars have carried out research on the physical and mechanical properties of poplar LVL. Liu *et al.* (2017) measured the tensile strength, compressive strength, and other physical and mechanical properties of poplar LVL, and found that poplar LVL had relatively uniform material properties and small variation, making it a suitable load-bearing material for building structures. Aydın *et al.* (2004) conducted physical and mechanical tests on poplar LVL made of two wood species (eucalyptus and beech) and two adhesives (urea formaldehyde and polyvinyl acetate) and found that the type of adhesives resulted in different strength characteristics of the LVL panels. Ido *et al.* (2010) tested the strength of LVL made from five wood species and

***bioresources*.com**

examined the lamination direction of veneer. It was found that the strength of the LVL material was related to the direction of the wood texture during assembly, except for radiata pine. Cui *et al*. (2016) found that the bending property of the LVL was considerably improved when the fiber line was implanted into the fast-growing poplar LVL. Meng *et al*. (2016) conducted mechanical tests on LVL made of poplar and eucalyptus with different veneer thicknesses and found that the modulus of elasticity (MOE), modulus of rupture (MOR), and horizontal shear of the LVL increased as the veneer thickness decreased. The experimental results showed that the poplar LVL, as an engineering wood material, exhibited stable material structure, good mechanical properties, high reliability, and low variability.

With the development of modern wood structures, the traditional connection methods used for the construction of wood structures may not meet modern performance requirements. To address this, researchers have, over years, conducted many studies on the mechanical properties of wood connections. He and Sun (2008) and Xu *et al*. (2011a) tested light wood truss joints connected by serrated plates, because the tooth plate connections could be the weak link of the whole truss. They analyzed the ultimate bearing capacity, the ultimate sliding capacity, and the ultimate tensile capacity of the serrated plates, and discovered that this kind of joint exhibits high ductility and low variability. Xu *et al*. (2011b) studied the bearing capacity of single bolted and group bolted connections in glulam under tension parallel to the grain direction of the wood and examined their failure modes and failure mechanisms. They found that the mechanical properties of a glulam-to-glulam single bolted connection was related to the thickness ratio of the glulam, and the mechanical properties of the glulam-to-glulam bolted connections were related to the number of bolted columns and the number of bolts in each column. Lu *et al*. (2016) designed and fabricated 9 glulam beam-column bolted joints, 7 of which were strengthened with self-tapping screws. They conducted monotonic and low cyclic loading tests and found that glulam beam-column bolted joints easily caused wood tearing damage, and the connections strengthened with self-tapping screws could effectively avoid cracking in the wood. Xu *et al*. (2009) experimentally and numerically studied the behaviour of dowel-type steel-to-timber joints tension loaded perpendicular to the grain. They found two primary types of failures, *i.e.*, splitting and embedding. They used the experimental results to validate a three-dimensional (3D) non-linear finite element model and found that the numerical results were in good agreement with the experimental results. Bader *et al*. (2016) investigated the behavior of connections made of slotted-in steels in LVL members bonded by single dowels with diameters of 12 and 20 mm with an aim to elucidate and subsequently simulate the load–displacement behavior of steel-dowel-LVL connections. They found that a pronounced nonlinear behavior of the single-dowel connections was observed for all load-to-grain directions. Sebastian *et al*. (2018) carried out double-shear tests on beech LVL-concrete composite connections based on the screw connectors singly inclined at either 45° or 90°. It was found that in the specimens with the same screw orientation, the longitudinal shear force was applied either in forward or reverse, because, in practice, concrete shrinkage, moisture-induced timber expansion and oscillatory, *e.g.*, seismic, or dynamic loads could induce the reversal force on the connection. Li (2005) studied the performance of the composite floor composed of pre-stressed, laminated slab and steel beam under uniform load bearing. The results showed that the composite floor can work together, and the rigid connectors can share most of the tensile stress in the concrete flange plate. Lu *et al*. (2016) conducted monotonic and low-cycle repeated loading tests on glulam beam-column-bolted joint specimens. They found that glulam

beam-column-bolted joints were prone to wood tearing damage, and applied self-tapping screws to reinforce the joint. The effect of the screw bite force effectively inhibited the cracking of the wood texture. Pathak and Charney (2008) simulated the lateral force of the floor and found that the nail connection was the primary source contributing to the in-plane flexibility, which was independent of the aspect ratio of the floor. Hassanieh and Valipour (2020) conducted the shear tests on three groups of wooden frames and discovered that the oriented strand board (OSB) panel thickness and nail size considerably affected the stiffness and strength. In summary, it could be seen from the above review that there have been limited studies on steel connections reinforced with self-tapping screws.

To fill this gap, nine full-scale connection specimens with three groups of different types of connectors were designed and fabricated. They were assembled and tested under concentrated loading, which was used to study the effect of the different connectors on the flexural performance, failure mode, bearing capacity, and stiffness. The results could provide a reference for the design and application of this type of connection in modern wooden structures.

EXPERIMENTAL

Design and Fabrication of the Specimens

Three types of poplar LVL-ribbed beam connections were designed and manufactured, each of which had 3 replicates, generating a total of 9 specimens. The design parameters of each type of connection are detailed in Table 1. Each specimen had a width of 1200 mm and a depth of 1200 mm. The inner part was composed of a primary beam and two secondary beams connected by connections to form an orthogonal ribbed beam joint. The section sizes of the three ribbed beams were 40 mm by 235 mm and the section size of the four ribbed beams of side fixing frame were 80 mm by 235 mm, which is illustrated in Fig. 1. The ribbed beams at the connection area were connected with three types of connections, *i.e.*, U-shape, T-shape, and L shape, as shown in Fig. 2, all of which were made of Q235B steel. The mechanical performance of the Q235B material was measured by Ma *et al.* (2018, 2019). According to relevant Chinese standards GB/T 50708-2012 (2012) "Technical code of glued laminated timber structures" and GB50005-2017 (2017) "Standard for design of timber structures", the screwing patterns and numbers of self-tapping screws were selected. The self-tapping screws were made of 304 stainless steel countersunk head screws with a specification of M4×20, with a yield strength of 205MPa and a tensile strength of 520MP. The sizes of the specimens are given in Fig. 2.

Table 1. Design Parameters of the 3 Types of Specimens

Specimen Code	Connector Form	Specimen Size (mm)	Replicate
JD1	U-shape	1200 x 1200	3
JD2	T-shape	1200 x 1200	3
JD3	L-shape	1200 x 1200	3
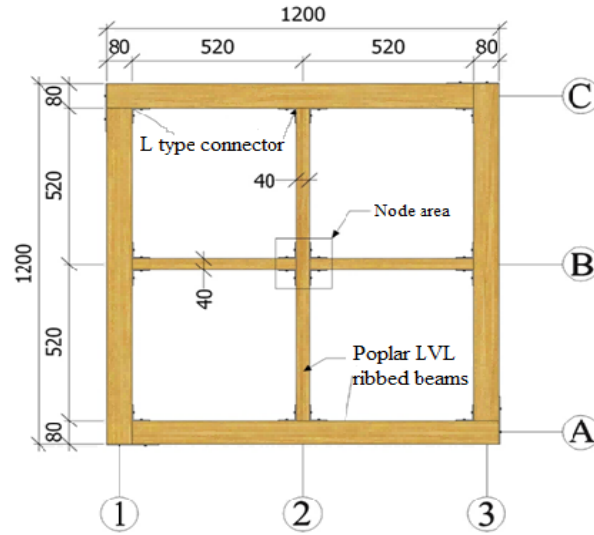
Fig. 1. Schematic of a connection specimen

(I) Lateral elevation   **(II) Front elevation**   **(III) Top view**   **(IV) 3D diagram**

(I) Lateral elevation   **(II) Front elevation**   **(III) Top view**   **(IV) 3D diagram**
(a) U-shape connector

(I) Lateral elevation   **(II) Front elevation**   **(III) Top view**   **(IV) 3D diagram**

(b) T-shape connector

(I) Left elevation   **(II) Front elevation**   **(III) Top view**   **(IV) 3D diagram**

(c) L-shape connector
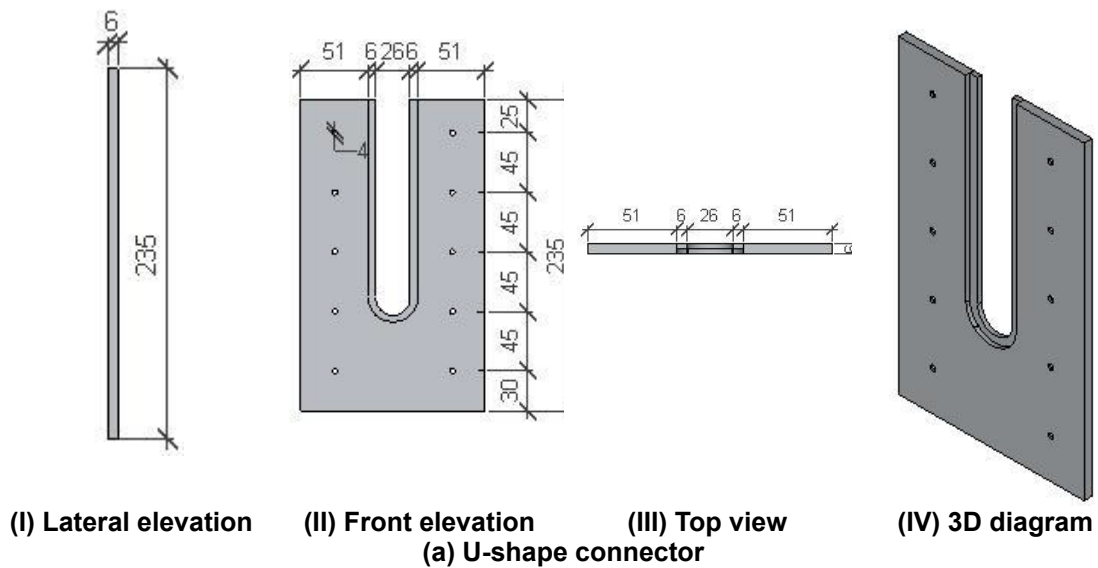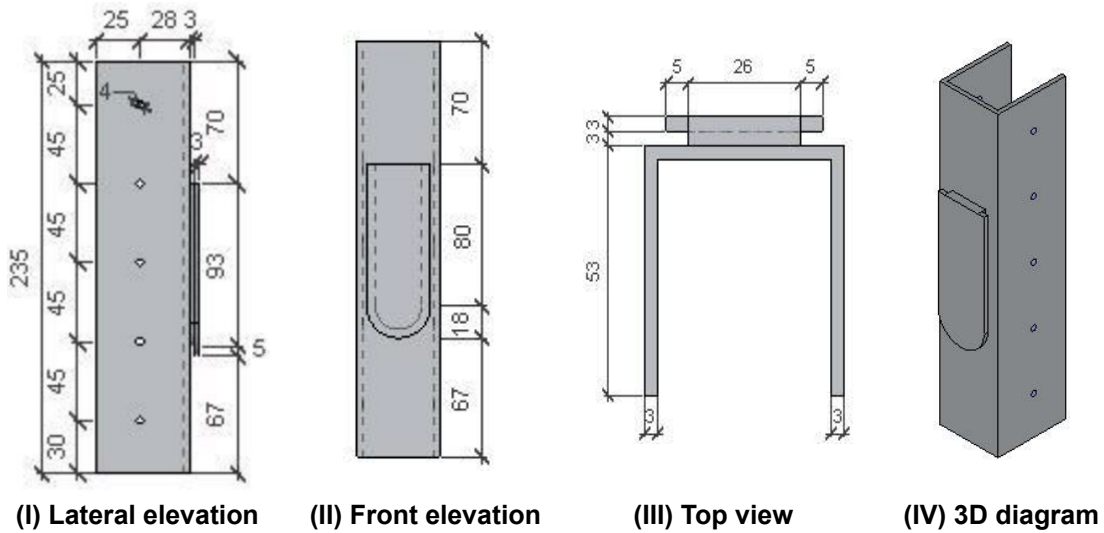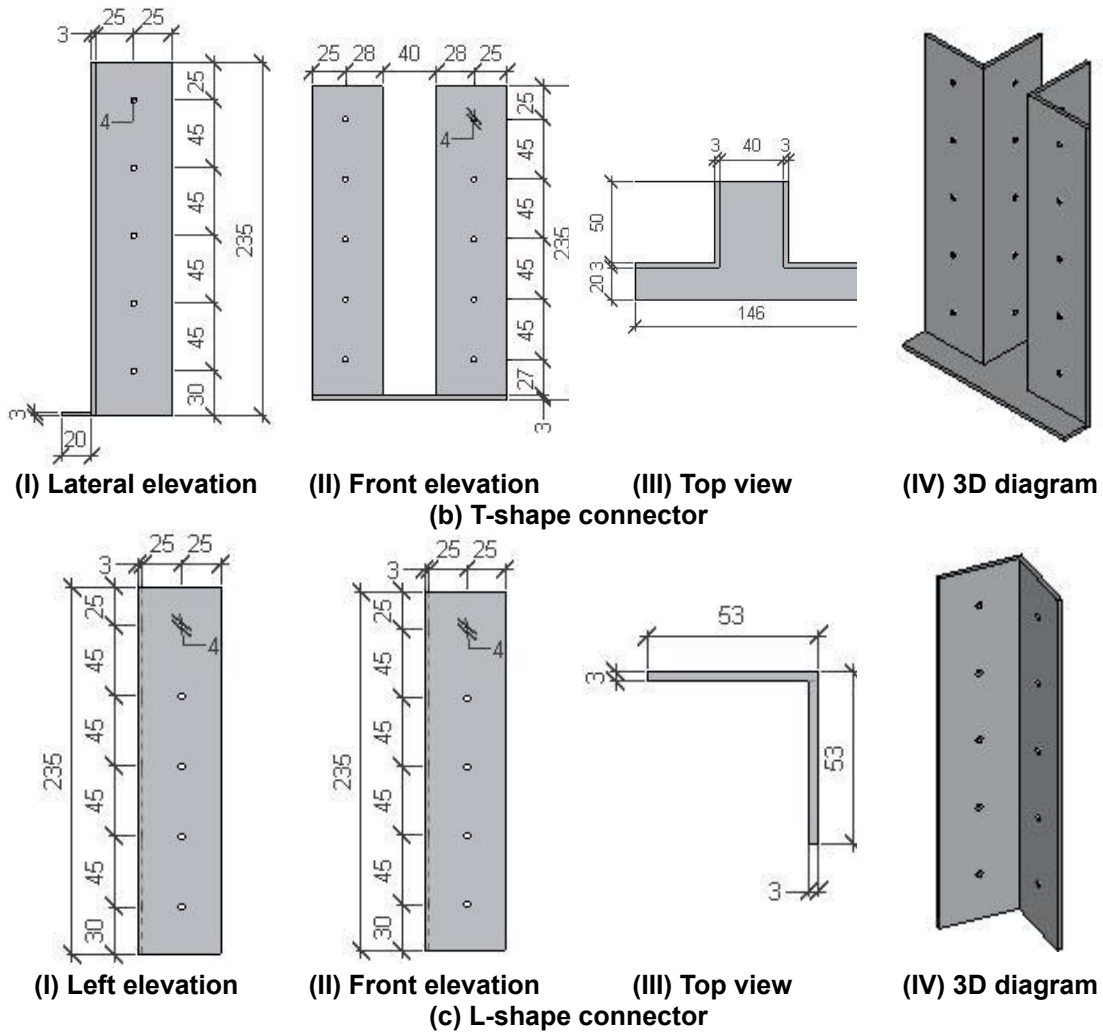
Fig. 2. Dimensions and construction of the connectors
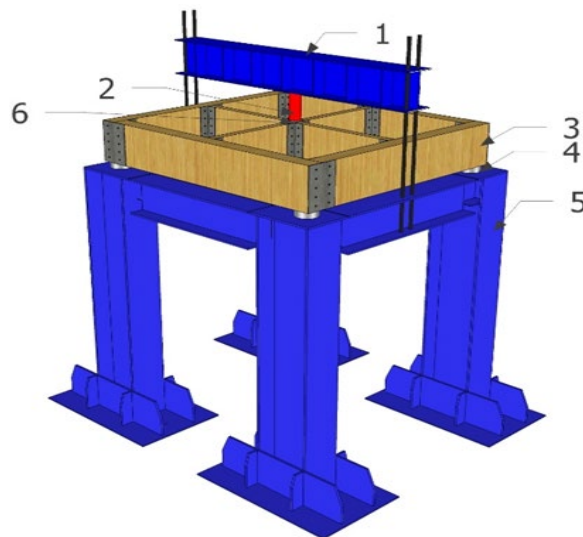
Fig. 3. Schematic of the experimental setup (Note: 1- Reaction frame; 2- Pressure jack; 3-Connector; 4-Pressure sensor; 5- H-Steel support; and 6-Four ribbed beam specimen)

Material Properties of Poplar Laminated Veneer Lumber (LVL)

The physical and mechanical properties of the poplar LVL were determined in a previous study by the author (Liu *et al.* 2017). The average moisture content of the poplar LVL was 13.1% and the average density was 0.57 g/cm^3. The mechanical properties of the poplar LVL are listed in Table 2. These quantities were previously tested by the authors as well (Liu *et al.* 2017).

Table 2. Material Properties of Poplar Laminated Veneer Lumber (LVL)

W (%)	ρ (g/cm^3)	E1 (MPa)	E2 (MPa)	E3 (MPa)	E4 (MPa)	P1 (MPa)	P2 (MPa)	P3 (MPa)	P4 (MPa)
13.1	0.570	11073	1630	602	9720	27.8	10.4	4.3	39.4

* *W* is the average moisture content of poplar LVL; *ρ* is the average density of the poplar LVL; E_1 is the modulus of elasticity in the parallel to the grain direction; E_2 is the modulus of elasticity in the radial direction; E_3 is the modulus of elasticity in the tangential direction; E_4 is the tensile modulus of elasticity in the parallel to the grain direction; P_1 is the compressive strength in the parallel to the grain direction; P_2 is the compressive strength 45° to the parallel to the grain direction; P_3 is the transverse grain compressive strength; and P_4 is the tensile strength in the parallel to the grain direction

Test Setup and Loading Scheme

A hydraulic jack was used to apply a concentrated load at the mid-span of a ribbed beam connection. The testing procedure referred to the methods for testing timber structures stipulated in the Chinese standard GB/T50329-2012 (2012) and ASTM E2322 (2015). The loading setup is shown in Fig. 3. First, the ultimate load of a specimen was estimated according to the formulas for calculating the shear bearing capacity and compression failure bearing capacity of a pin fastener provided in the Chinese standard GB50005-2017 (2017). A preload was applied to the specimen before actually starting the loading. The load was kept for 5 min when the load was added to 5% of the ultimate load and then unloaded. All measuring equipment was zeroed prior to loading. A hierarchical loading scheme was followed, *i.e.*, the first stage was loaded with approximately 10% of the ultimate load, and the second stage was loaded with approximately 5% of the ultimate load until it was damaged. The holding time for each loading stage was 5 min.

Instrumentation

In order to measure the changes of the connection deflections and rib strains of each specimen during the loading process, the displacement meters and strain gauges were arranged at the bottom of the connection rib beam, and load cells were placed at the end of the rib beam and the corner of a specimen to measure the load distribution of a connection rib specimen. The arrangement of the measuring points is shown in Fig. 4, among which W1 through W7 represent the displacement meter numbers, C1 through C7 represent the strain gauge numbers (note: the JD2 specimens were not measured at the measurement points C2, C5, and C6 due to the connection construction), and N1 through N8 represent the load cell number.
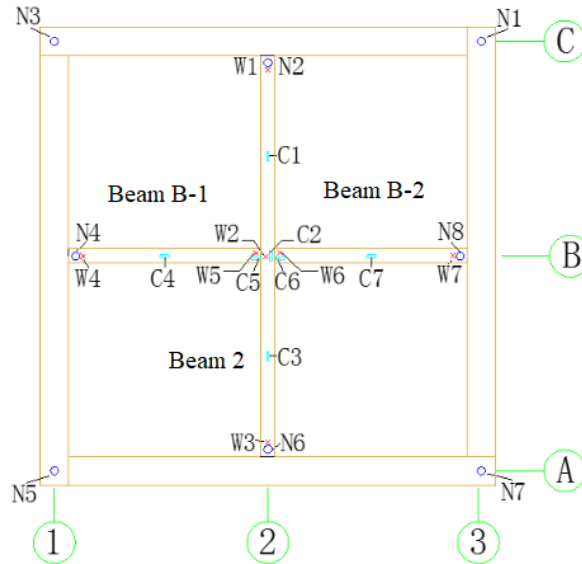
Fig. 4. Arrangement of the measuring locations

GENERAL BEHAVIOR AND FAILURE PATTERN

JD1 specimen (U-shaped type)
  When loaded to 21 kN, the specimen emitted a slight squeezing sound. When the load reached 33 kN, a crack began to appear between the plug and the slot of a connector, and the crack continued to grow as the load increased.

(a) Slip at the end of Beam 2

(b) Cracking of the LVL

(c) Separation between the end of Beam B-2 and the side beam

(d) Pull-out of the self-tapping screws at the connection

Fig. 5. The failure morphology of specimen JD1

When the load reached 51 kN, the self-tapping screws between Beam 2 and the slot were slightly pulled out. When the load reached 55 kN, the end 2 of the beam slid down, and the subsidence distance reached 4 mm, as shown in Fig. 5a. When the load reached 60 kN, the wood in contact with the load cell was crushed, as shown in Fig. 5b. At this time, the end of Beam B-2 was separated from the 3-axis side beam, and the clearance reached 10 mm, as shown in Fig. 5c. When the final load reached approximately 68 kN, the self-tapping screws between Beam 2 and the slot was pulled out, and the connection separation gap reached approximately 14 mm, making the specimen fully fail, as shown in Fig. 5d.

JD2 specimen (T-shaped type)

Before the load was loaded to 42 kN, the specimen showed no obvious failure. When the load reached approximately 52 kN, the specimen emitted a slight squeezing sound. When the load reached approximately 55 kN, the two T-type connectors at the connection began to separate. As the load continued to increase, the end 2 of the beam connected to the axis side of Beam A appeared to slide down, as shown in Fig. 6a.

(a) Slip at the end of Beam 2

(b) Slip at the right end of Beam B-2

(c) Separation between the connectors

(d) Separation between the connectors
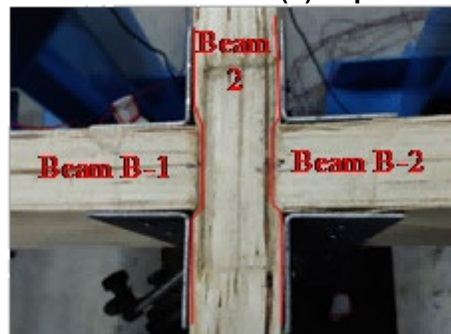
(e) crushing of Beam 2 against Beams B-1 and B-2

Fig. 6. The failure morphology of specimen JD2

At this time, the right end of Beam B-2 appeared to sag 5 mm at the connection along the axis side of Beam 3, as shown in Fig. 6b. When the load reached approximately 65 kN, the gap between the end of Beam B-1 and Beam B-2 at the connection and Beam 2 was approximately 10 mm, as shown in Fig. 6c, and the spacing between the two connectors reached approximately 7 mm, as shown in Fig. 6d. Finally, the specimen failed.

JD3 specimen (L-shaped type)

When the load reached approximately 12 kN, the specimen produced a slight sound due to the crushing of the wood. When the load reached approximately 27 kN, Beam 2 produced a fiber tearing sound in the wood, and the right end of Beam B-1 and the left end of Beam B-2 began to sag. When the load reached approximately 36 kN, obvious deflection occurred at the midpoint of Beam 2. When the load reached approximately 42 kN, the tearing sound of the wood fibers became quite loud, and the self-tapping screws at the lower part of the connector at the 2 connections of the beam were pulled out, as shown in Fig. 7a. As the load continued to increase, the support at the end of Beam 2 began to slide down. When the load reached approximately 50 kN, oblique cracks appeared at the right upper end of Beam B-2 where it met the connector, and the wood was pulled apart, as shown in Fig. 7b. When the final load reached approximately 60 kN, the screws at the lower end of Beam 2 were pulled out, and the gap between Beam 2 and Beam B-1 was approximately 10 mm, as shown in Fig. 7c. Meanwhile, the end of Beam 2 connected to the axis side beam of A was compressed approximately 3 mm, and the wood at the upper end of Beam 2 was torn, as shown in Fig. 7d. The specimen finally failed.

(a) Pull-out of the lowest screw in Beam 2

(b) Oblique cracking at the right upper end of Beam B-2

(c) Pull-out of the screws at the lower end of Beam B-1

(d) Crushing of the wood at the end of Beam 2
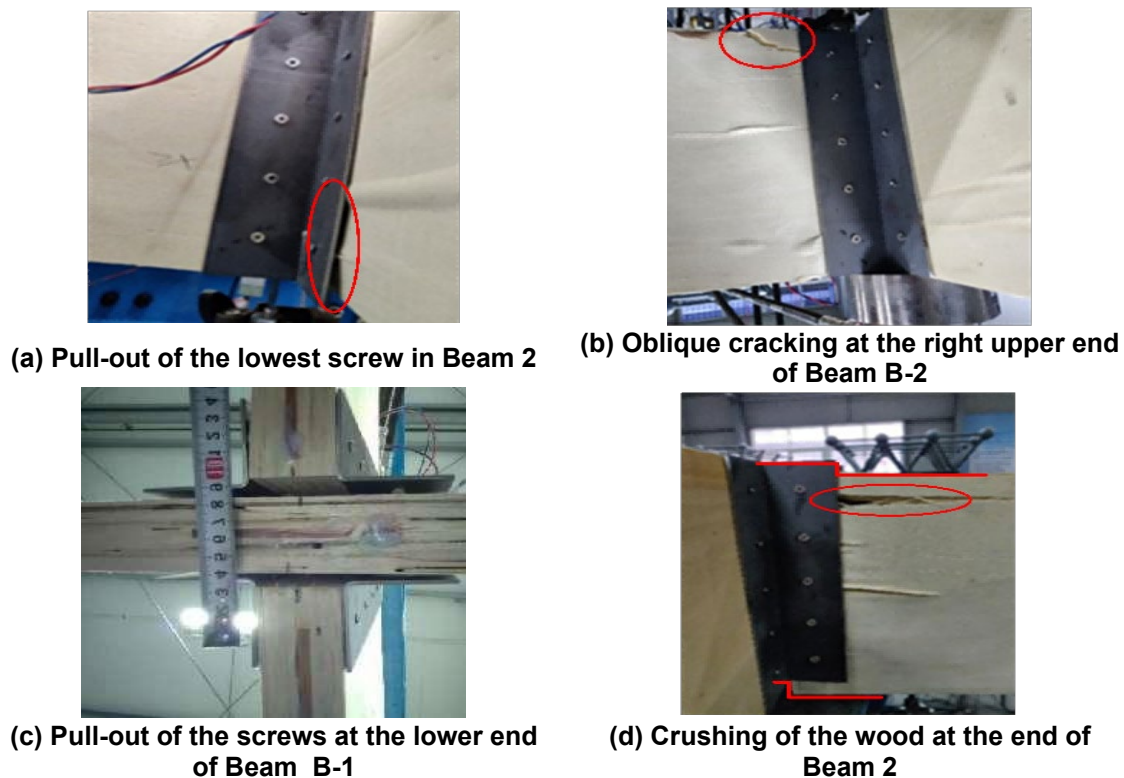
Fig. 7. The failure morphology of specimen JD3

Analysis of failure

According to the above description on the failure of each specimen, the overall initiation and propagation of failure in a specimen was as follows: (1) pull-out of the self-tapping screws at the lower part of the specimen; (2) separation of the connection and the ribbed beam; (3) crushing of the wood at the end of the ribbed beam; and (4) failure. In summary (as shown in Fig. 8), first of all, the screws connected on both sides of the lower end of Beam 2 at the connection were pulled out. Some of the screws began to fracture, the bearing capacity of the connection began to decrease, the deflection at the connection increased, the end of each rib beam was stressed, the end of the beam slid down, and finally the end wood in contact with the support was crushed.

| (a) Separation of a | (b) Nails bended in | (c) End sag and wood crushing in the |
| connection | a connection | end of a beam |
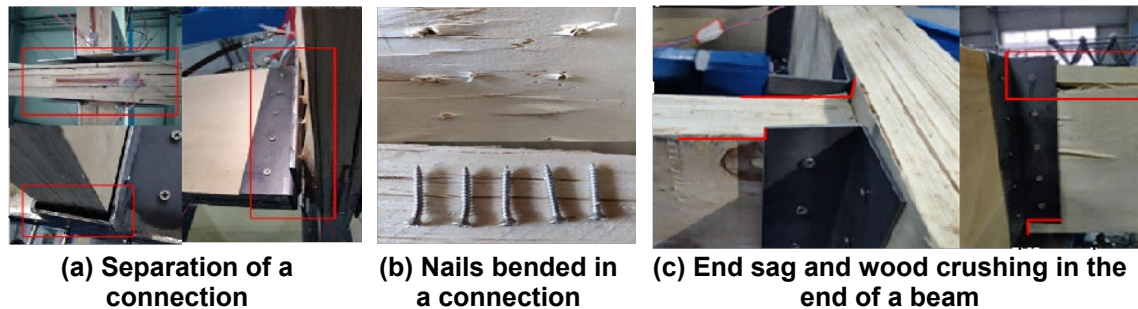
Fig. 8. Failure evolution of a nodal specimen

ANALYSIS AND DISCUSSION

Load-displacement Response

The load-displacement curve of each specimen was plotted (Fig. 9). The displacement linearly increased as the load increased at the initial stage of loading. When the load reached 80% of the ultimate load, the displacement growth rate of the specimen was accelerated, and the load-displacement curve becomes nonlinear. When the load continues to increase, the displacement growth rate was further accelerated due to the pull-out of some screws in the specimens. Before the failure of a specimen, the ductile behavior appears obvious. Throughout the whole loading process, it is not surprising that the midpoint of a specimen exhibited the maximum displacement. During the loading process, some screws in the mid-span connection area were pulled out, weakening the connection performance of the specimen, and reducing the load transfer from the 2-axis ribbed beam to the B axis ribbed beam. During the course of the loading process, some screws were pulled out from the connection, reducing its load capacity. Therefore, the displacements at the supports of Beam B-1 (point W4) and Beam B-2 (point W7) were smaller than the displacements at the support of Beam 2 (points W1 and W3). For specimens JD1 and JD3, the displacements of the ribbed ends in two directions were 6.10 mm and 5.49 mm, respectively, while for type JD2, the displacement of the ribbed ends in two directions was only 1.87 mm. This was because of the presence of the T-plate at the bottom of specimen type JD2, which increased the overall deformation performance of the connections.

(a) Load-displacement curves of the JD1 specimens

(b) Load-displacement curves of the JD2 specimens

(c) Load-displacement curves of the JD3 specimens
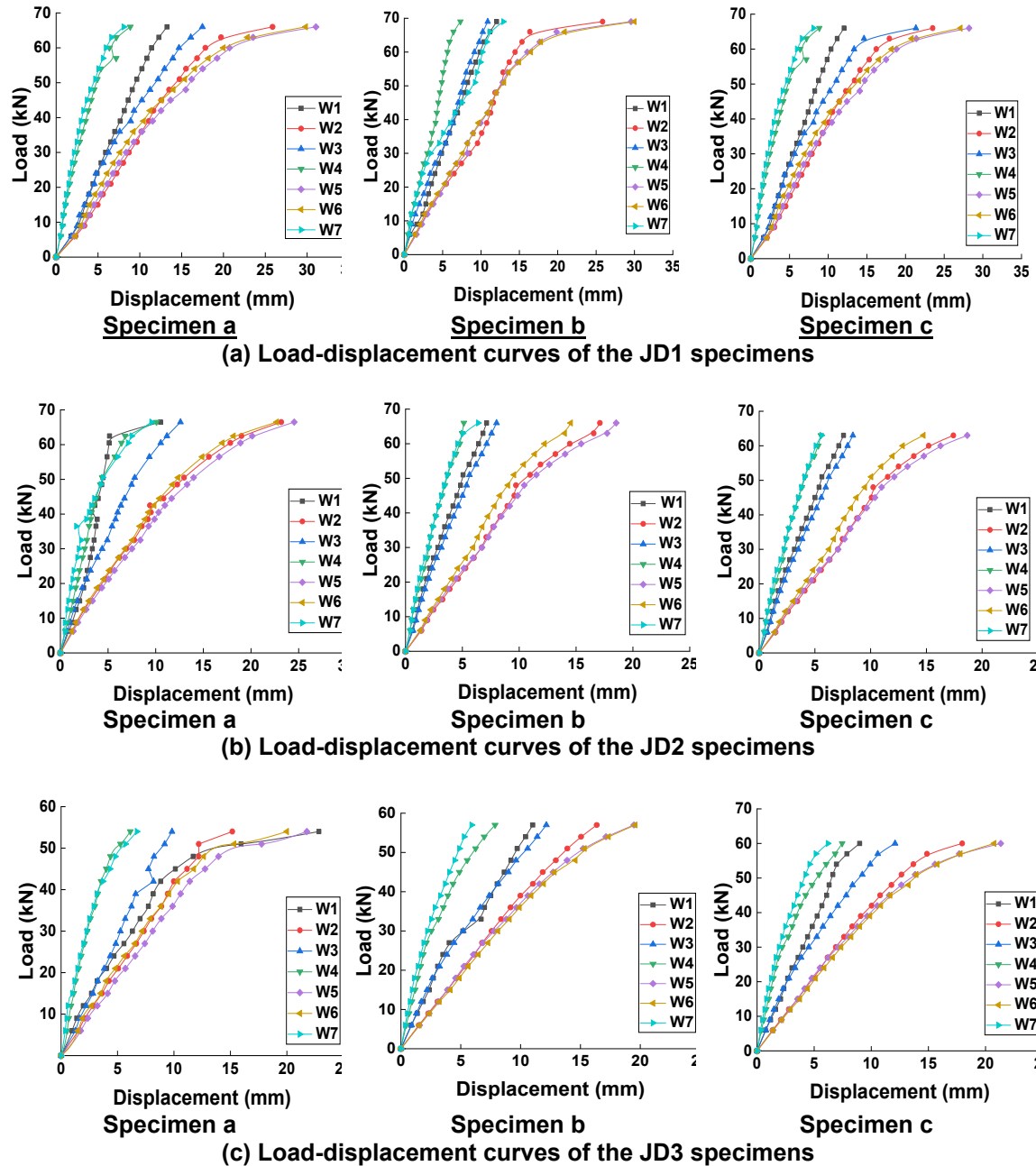
Fig. 9. Load-displacement curves of three types of specimens tested

Load-strain curves

The load-strain curve at each measuring point is shown in Fig. 10. It can be found that these curves almost linearly increased throughout the whole loading stage. Under load, the strain change at the middle point of Beam 2, *i.e.*, point C2, was the largest, and as the load increased, the strain change at point C2 began to show a nonlinear increase. For Beam B-1 and Beam B-2, the strains at their midpoints C4 and C7 and the end points C5 and C6 of the beam were very small. This could be because the self-tapping screws at these points were pulled out, and the bottom end of Beams B-1 and B-2 were detached from Beam 2 near the connection points.
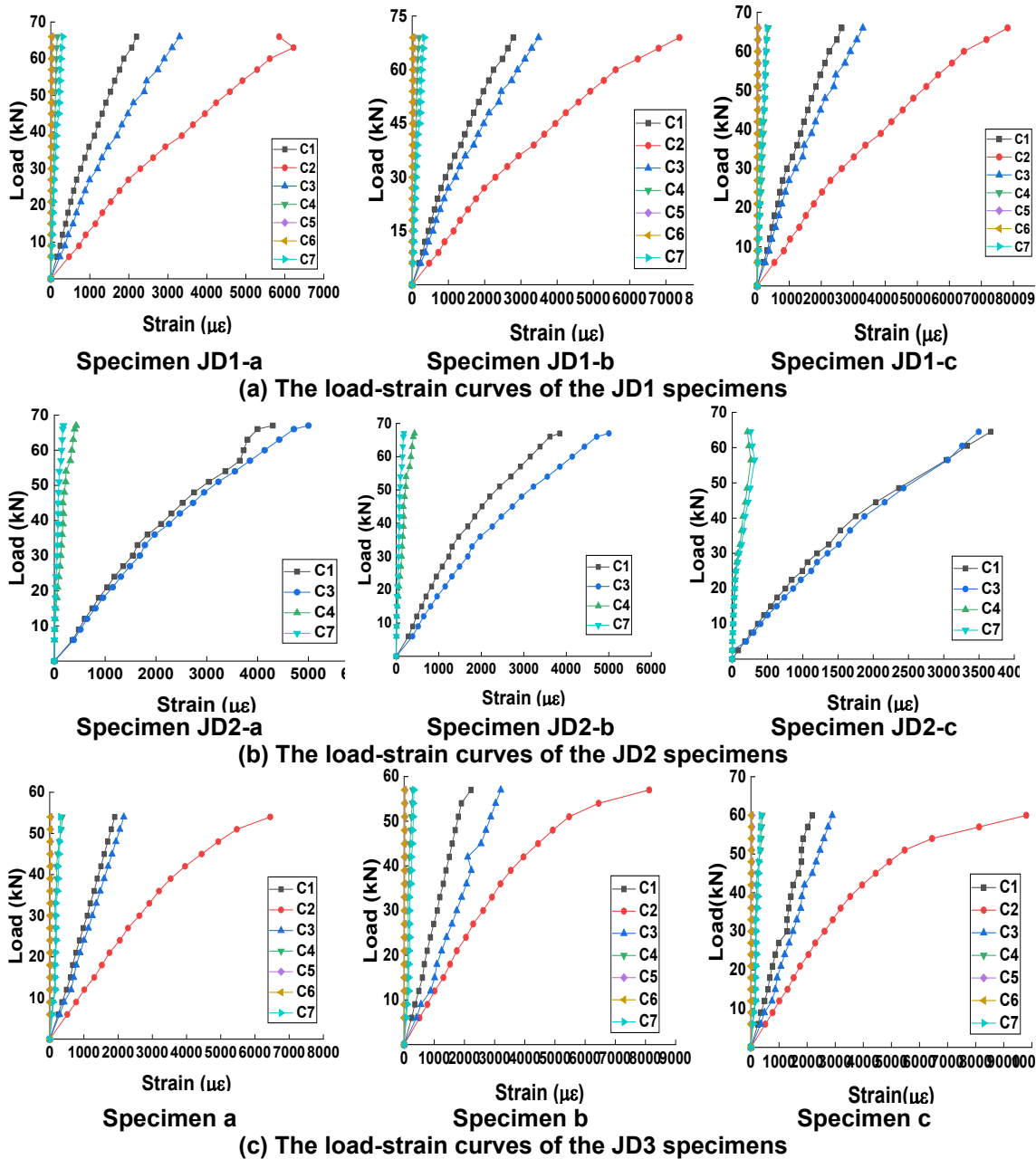
Fig. 10. Load-strain curves at various points of all the specimens tested

Load distribution curves

From the load-displacement curve in Fig. 9, it can be seen that before 0.8 of the ultimate load of the specimen (P_{max}), it basically behaved in the linear elastic way. Therefore, the slope of the straight line corresponding to $0.1P_{max}$ and $0.8P_{max}$ was used to calculate the bending stiffness of each specimen.

Throughout the course of the loading process, load cells were used to measure the load values at the end of the points of a ribbed beam, *i.e.*, N2, N4, N6, and N8, and at the four corners, *i.e.*, N1, N3, N5, and N7, of all three types of specimens. The load distribution curves are shown in Fig. 11. It can be seen that the bearing reaction linearly increased, during the whole loading process, with the increase of the load. The values of the bearing

reaction at the four corners of the specimen closely varied, while the bearing reaction at the end of the connection-ribbed beam appeared discrete with the increase of the load. As the load continued to increase, some screws in the connections began to fail and the connections became detached, which reduced the overall performance of the connections. The load distributed on Beam B-1 and Beam B-2 decreased, and the load value at the end of Beam 2 increased faster than the load value of Beam B-1 or Beam B-2.

(a) Load distribution curves of the JD1 specimens

(b) Load distribution curves of the JD2 specimens

(c) Load distribution curves of the JD3 specimens
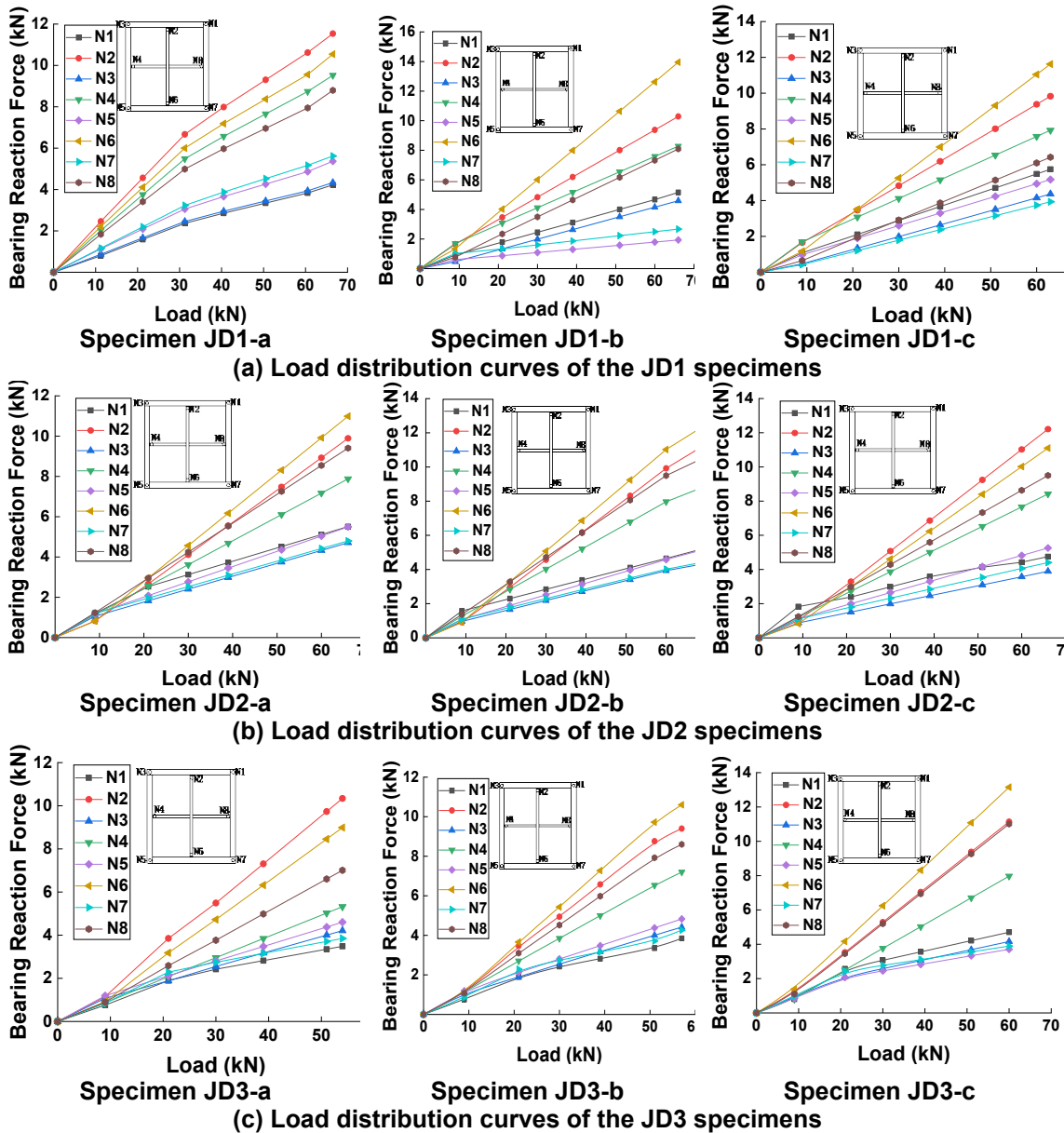
Fig. 11. The load distribution curves at various points of all the specimens tested

The load distribution ratio of the nodal ribbed beams of a specimen is defined as the ratio of the load at the end of the 2-axis and B-axis ribbed beams to the total load, which is shown in Table 3.

The load value distributed at the end of Beam 2 of each specimen was the largest, which accounted for approximately 36% of the total load. For different specimens, their

load distributions at the ends of the ribbed beams in both directions of the connections were different. A 3.2% difference in the average load distribution ratio of the JD2 specimens was discovered (the smallest among all three types). The difference in the load distribution of the other two types of specimens, *i.e.*, JD1 and JD3, in both directions was similar, within 10%. Based on the deformation at failure of a specimen, it was found that specimen JD2 had the lowest degree of failure, since this group had the best degree of integrity, while specimens JD1 and JD3 showed more serious failure, which had a big impact on the load distribution at the connection.

Table 3. Load Distribution Ratio of the Ribbed Beam Connection Specimens

Specimen		Number of Points Measured			
		N2	N4	N6	N8
JD1	Specimen a	19.5%	16.0%	17.6%	14.6%
	Specimen b	18.9%	16.3%	23.0%	13.4%
	Specimen c	18.5%	16.0%	19.5%	10.8%
	Average	*18.9%*	*16.1%*	*20.1%*	*12.9%*
JD2	Specimen a	14.8%	13.3%	13.3%	15.5%
	Specimen b	15.9%	14.2%	17.5%	16.6%
	Specimen c	17.9%	13.7%	16.1%	15.2%
	Average	*16.2%*	*13.8%*	*15.6%*	*15.8%*
JD3	Specimen a	19.7%	10.9%	16.8%	13.6%
	Specimen b	16.6%	13.3%	18.0%	15.3%
	Specimen c	16.9%	12.0%	20.0%	16.5%
	Average	*17.7%*	*12.1%*	*18.3%*	*15.2%*

Analysis on the flexural capacity

According to the test results, the flexural rigidity value, the ultimate bearing capacity, and the maximum deflection displacement at failure of each type specimens are shown in Table 4.

Table 4. Ultimate Bearing Capacity, Deflection at Failure, and Flexural Rigidity of the Specimens Tested

Specimen code	Ultimate Bearing Capacity (kN)	Average (kN)	Deflection at Failure (mm)	Average (mm)	Bending stiffness (N/mm^{-1})	Average (N/mm^{-1})
JD1-a	66.3		31.1		3445	
JD1-b	69.1	67.3	30.0	29.8	3533	3589
JD1-c	66.4		28.2		3789	
JD2-a	67.2		24.5		4337	
JD2-b	66.0	65.5	18.5	20.6	4474	4354
JD2-c	63.4		18. 7		4250	
JD3-a	54.5		22.8		4086	
JD3-b	57.7	57.5	19.6	21.2	3957	4132
JD3-c	60.3		21.3		4353	

It can be seen that specimen JD1 had a maximum bearing capacity of 67.3 kN; however, it also had the lowest overall stiffness or a large deformation. This could be attributed to the contribution of the mechanical interlock force existing in the connections. Compared with specimen JD2, the stiffness was 21.3% lower under similar bearing

bioresources.com

capacity conditions. Compared with specimen JD3, the bearing capacity was 17.0% higher, but the stiffness was 15.1% lower than specimen JD3. Due to the presence of a T-plate at the bottom of the connection in specimen JD2, the bearing capacity of specimen JD2 increased by 13.9%, but the displacement and stiffness values of specimen JD2 were similar. By comparing the experimental results of the three types of poplar LVL ribbed-beam connection specimens, it can be seen that specimen JD3 was close to specimen JD2 in terms of the mechanical performance, which was better than specimen JD1. However, it should be pointed out that the fabrication of specimen JD2 was not as easy as specimen JD3. According to the failure modes of the specimens discussed above, the primary failure mode of specimens JD1 and JD3 was the failure of the screws at the end of the ribbed beams and connection regions. The failure position of the screws is shown in Fig. 12. For specimen JD2, the failure of the self-tapping screws at the end of the ribbed beam and crushing at the top of the middle point of Beam 2 primarily occurred, as shown in Fig. 13. Referring to the Chinese standard GB50005-2017 (2017), the formulas for calculating the shear bearing capacity and compression bearing capacity of a pin fastener were used. The calculated failure loads of each specimen are shown in Table 5, from which it can be seen that the calculated values are in good agreement with the actual values from the experiment.

The design value (Z_d) stands for the bearing capacity of each shear face, as calculated by Eq. 1,

$$Z_d = C_m C_n C_t K_g Z \tag{1}$$

where C_m is the moisture content adjustment coefficient; C_n is the adjustment coefficient of design service life; C_t is the temperature adjustment coefficient; K_g is the group bolt combination coefficient; and Z is the reference design value of bearing capacity, which is calculated according to Eq. 2,

$$Z = k_{min} t_s d f_{es} \tag{2}$$

where k_{min} is the minimum effective length coefficient of the bearing capacity of a pin groove of a single shear connection or the thinner side member of a double shear connection; t_s is the thickness of a thinner member or side member (mm); d is the diameter of a pin shaft fastener (mm); and f_{es} is the standard value of the bearing strength of a member pin groove.

The maximum compressive load of a beam was calculated according to Eq. 3,

$$P_{max} = \sigma_w b t \tag{3}$$

where σ_w is the compressive strength (MPa) of wood in the parallel to the grain direction at a given moisture content (W); P_{max} is the failure load (N); b is the specimen width (mm); and t is the specimen thickness (mm).

Table 5. Number of Failed Self-Tapping Screws and Failure Load Calculated

Specimen Code	Z_d (kN)	Number of Failed Screws		P_{max} (kN)	Failure Load (kN)	
		End of Ribbed Beam	Connection Area		Calculated Value	Tested Value
JD1	1.29	40	12	-	67.1	67.3
JD2	1.29	40	-	17.8	69.4	65.5
JD3	1.29	40	4	-	56.8	57.5
Note: Z_d is the calculated value of the shear capacity of a single screw considering the group bolt coefficient; and P_{max} is the load of the top of the ribbed beam for specimen JD2 under compression.						

bioresources.com

(a) Failure location of the screws at the end of a ribbed beam

(b) Failed screws (red) in connection area of a JD1 specimen

(c) Failed screws (red) in connection area of a JD3 specimen
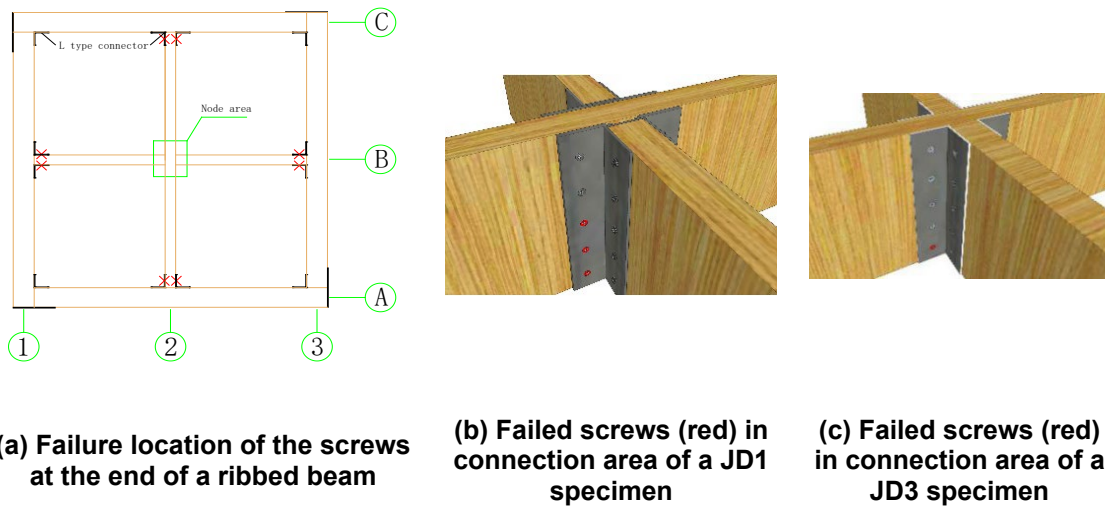
Fig. 12. The schematic diagrams showing the failure locations of self-tapping screws
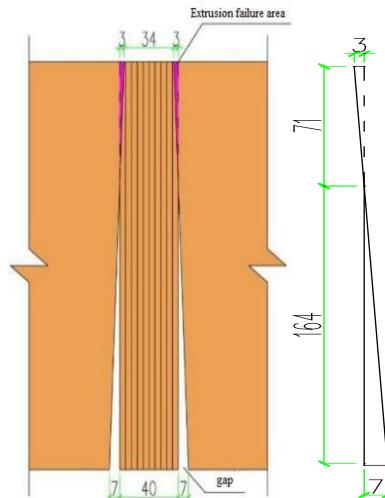
Fig. 13. Schematic showing compressive stresses at the top of a ribbed beam of a JD2-type specimen

CONCLUSIONS

1. The three types of ribbed beam connection specimens designed, fabricated, and tested showed good connecting performance, and ductile failure was observed, including the pull-out of partial self-tapping screws, crushing of the LVL at the end of the ribbed beam, and connection failure.

2. The load distribution along the ribbed beams in two directions of each specimen was different. The JD2-type specimens had the smallest variation (approximately 3.2%), while the JD1- and JD3-type specimens had a relatively larger difference but was still less than 10%. The JD2- and JD3-type specimens had similar stiffness, with a difference of only 5.1%, while the JD1-type specimens had the smallest stiffness, approximately 17.5% less than the stiffness of the JD2-type specimens, which had the largest deflection at failure.

3. The calculated ultimate bearing capacity of a connection specimen was proportional to the number of self-tapping screws.

4. The mechanical performance of the U-shaped connection specimens was poor, and the mechanical performance of the L-shaped connection specimens was similar to the mechanical performance of the T-shaped ones.

ACKNOWLEDGMENTS

REFERENCES CITED

ASTM E2322-03 (2015). "Standard test method for conducting transverse and concentrated load tests on panels used in floor and roof construction," ASTM International, West Conshohocken, PA.

Aydın, İ., Çolak, S., Çolakoğlu, G., and Salih, E. (2004). "A comparative study on some physical and mechanical properties of laminated veneer lumber (LVL) produced from beech (*Fagus orientalis* Lipsky) and eucalyptus (*Eucalyptus camaldulensis* Dehn.) veneers," *Holz als Roh- und Werkstoff* 62(3), 218-220. DOI: 10.1007/s00107-004-0464-3

Bader, T. K., Schweigler, M., Serrano, E., Dorn, M., Enquist, B., and Hochreiner, G. (2016). "Integrative experimental characterization and engineering modeling of single-dowel connections in LVL," *Construction and Building Materials* 107, 235-246. DOI: 10.1016/j.conbuildmat.2016.01.009

Cui, J., Han, S., Yuankang, H., and Jiang, G. (2016). "Influence of glass fiber implantation on the mechanical properties of poplar laminated veneer lumber," *Journal of Forestry Engineering* 2016(5), 40-44. DOI: 10.13360/j.issn.2096-1359.2016.05.008

GB 50005-2017 (2017). "Standard for design of timber structures," Standardization Administration of China, Beijing, China.

GB/T 50708-2012 (2012). "Technical code of glued laminated timber structures," Standardization Administration of China, Beijing, China.

GB/T 1938-2009 (2009). "Method of testing in tensile strength parallel to grain of wood," State Forestry Administration, Beijing, China.

GB/T50329-2012 (2012). "Standard for test methods of timber structures," China Construction Industry Press, Beijing, China.

Hassanieh, A., and Valipour, H. (2020). "Experimental and numerical study of OSB sheathed-LVL stud wall with stapled connections," *Construction and Building Materials* 233, 1-16. DOI: 10.1016/j.conbuildmat.2019.117373

He, M., and Sun, Y. (2008). "Test and load-bearing capacity of metal plate connected joint," *Special Structures* 25(1), 1-5.

Ido, H., Nagao, H., Kato, H., Miyatake, A., and Hiramatsu, Y. (2010). "Strength properties of laminated veneer lumber in compression perpendicular to its grain," *Journal of Wood Science* 56(5), 422-428. DOI: 10.1007/s10086-010-1116-3

Li, H. (2005). *Research on Mechanical Behavior of New Composite Slabs under Vertical Uniform Load*, Master's Thesis, Wuhan University, Wuhan, China.

Liu, Y., Diao, H., and Yang, G. (2013). *Architecture and Structure of Wood Structure*, China Forestry Press, Beijing, China.

Liu, Y., Wang, H., Ding, P., and Song, Y. (2017). "Physical and mechanical properties of Italian poplar veneer plywood," *Forest Products Industry* 44(02), 12-16.

Lu, W., Sun, H., and Liu, W. (2016). "Experimental study on behavior of bolted glulam beam-to-column connections strengthened by self-tapping screws," *Journal of Building Structures* 37(4), 80-86. DOI: 10.14006/j.jzjgxb.2016.04.011

Ma, H., Wang, J., Lui, E. M., Wan, Z., and Wang, K. (2019). "Experimental study of the behavior of beam-column connections with expanded beam flanges," *Steel and Composite Structures* 31(3), 319-327. DOI: 10.12989/scs.2019.31.3.319

Ma, H., Zhao, Y., Wang, Z., Chen, Y., and Wang, K. (2018). "Hysteretic behaviour analysis of new beam-column connections with expanded flange of steel frame," *Journal of Yangzhou University (Natural Science Edition)* 21(1), 50-55. DOI: 10.19411/j.1007-824x.2018.01.012

Meng, F., Ling, W., Lun, Y., and Ji, Y. (2016). "Effect of thicker veneers on properties of laminated veneer lumber," *China Wood Industry* 2016(3), 5-8.

Pathak, R., and Charney, F. A. (2008). "The effects of diaphragm flexibility on the seismic performance of light frame wood structures," in: *The 14th World Conference on Earthquake Engineering*, 12-17 October, Beijing, China, pp. 1-8.

Sebastian, W. M., Piazza, M., Harvey, T., and Webster, T. (2018). "Forward and reverse shear transfer in beech LVL-concrete composites with singly inclined coach screw connectors," *Engineering Structures* 175, 231-244. DOI: 10.1016/j.engstruct.2018.06.070

Xiong, H., Kang, J., and He, M. (2018). *Light Wood Frame Construction*, Tongji University Press, Shanghai, China.

Xu, B. H., Bouchaïr, A., Taazount, M., and Vega, E. J. (2009). "Numerical and experimental analyses of multiple-dowel steel-to-timber joints in tension perpendicular to grain," *Engineering Structures* 31(10), 2357-2367. DOI: 10.1016/j.engstruct.2009.05.013

Xu, D., Liu, W., Zhou, D., and Xi, A. (2011a). "Experimental and statistical analysis on load carrying capacity of metal plate with orthogonal oriented teeth in light wood frame construction," *Journal of Tongji University (Natural Science)* 37(12), 1581-1585.

Xu, D., Liu, W., Zhou, D., and Xi, A. (2011b). "Experimental study of bolted glued timber-to-timber joints," *Journal of Building Structures* 32(7), 93-100. DOI: 10.14006/j.jzj-gxb.2011.07.014